Acta Crystallographica Section F
Structural Biology and Crystallization Communications
ISSN 1744-3091

Structure of *Aeropyrum pernix* fibrillarin in complex with natively bound *S*-adenosyl-L-methionine at 1.7 Å resolution

Udesh de Silva,[a]‡ Zhaoli Zhou[b]‡ and Bernard A. Brown II[c]*

[a]Laboratory of Molecular Biology, National Institute of Diabetes and Digestive and Kidney Diseases, National Institutes of Health, 9000 Rockville Pike, Bethesda, MD 20892, USA, [b]Department of Chemistry and Chemical Biology, Cornell University, 214 Bard Hall, Ithaca, NY 14853, USA, and [c]Womble Carlyle Sandridge and Rice LLP, One West Fourth Street, Winston-Salem, NC 27101, USA

‡ These authors contributed equally to this work.

Correspondence e-mail: bebrown@wcsr.com

Received 18 April 2012
Accepted 12 June 2012

PDB Reference: fibrillarin–*S*-adenosyl-L-methionine complex, 4df3.

Fibrillarin is the key methyltransferase associated with the C/D class of small nuclear ribonucleoproteins (snRNPs) and participates in the preliminary step of pre-ribosomal rRNA processing. This molecule is found in the fibrillar regions of the eukaryotic nucleolus and is involved in methylation of the 2′-O atom of ribose in rRNA. Human fibrillarin contains an N-terminal GAR domain, a central RNA-binding domain comprising an RNP-2-like superfamily consensus sequence and a catalytic C-terminal helical domain. Here, *Aeropyrum pernix* fibrillarin is described, which is homologous to the C-terminal domain of human fibrillarin. The protein was crystallized with an *S*-adenosyl-L-methionine (SAM) ligand bound in the active site. The molecular structure of this complex was solved using X-ray crystallography at a resolution of 1.7 Å using molecular replacement with fibrillarin structural homologs. The structure shows the atomic details of SAM and its active-site interactions; there are a number of conserved residues that interact directly with the cofactor. Notably, the adenine ring of SAM is stabilized by π–π interactions with the conserved residue Phe110 and by electrostatic interactions with the Asp134, Ala135 and Gln157 residues. The π–π interaction appears to play a critical role in stabilizing the association of SAM with fibrillarin. Furthermore, comparison of *A. pernix* fibrillarin with homologous structures revealed different orientations of Phe110 and changes in α-helix 6 of fibrillarin and suggests key differences in its interactions with the adenine ring of SAM in the active site and with the C/D RNA. These differences may play a key role in orienting the SAM ligand for catalysis as well as in the assembly of other ribonucleoproteins and in the interactions with C/D RNA.

1. Introduction

The small nucleolar RNAs (snoRNAs) are essential for ribosome biogenesis, facilitating the folding and cleavage of pre-ribosomal RNA transcripts and guiding the modification of ribosomal RNA nucleotides. These include C/D box members that guide methylation and H/ACA members that guide pseudouridylation in rRNA molecules. The C/D box snoRNAs direct 2′-*O*-methylation of ribose in rRNAs *via* ribonucleoprotein (RNP) complexes, which are evolutionarily ancient nucleotide-modification machines that are found in both eukaryotes and archaea. In eukaryotes the C/D box RNAs associate with a common set of four core proteins to form asymmetric RNPs consisting of 15.5 kDa/Snu13p, Nop56, Nop58 and fibrillarin. In archaeal organisms only three core proteins, L7Ae, Nop56/58 and fibrillarin, are required for functional sRNPs. The fibrillarin molecule is the most abundant protein found in the fibrillar regions of the eukaryotic nucleolus. The early stages of pre-rRNA processing take place in the fibrillar region and it is also known that fibrillarin is essential for cell viability and for snoRNA and pre-rRNA processing (Eichler & Craig, 1994). It has been shown that point mutations in fibrillarin (Nop1p in *Saccharomyces cerevisiae*) can inhibit downstream steps in ribosome synthesis (Newton *et al.*, 2003).

Fibrillarin is a key protein component of the C/D box snoRNP family and is essential for the assembly of snoRNP particles and the stabilization of snoRNA (Caffarelli *et al.*, 1998). The crystal structure of the fibrillarin homolog from *Methanococcus jannaschii* contains an *S*-adenosyl-L-methionine (SAM) binding region in the C-terminal

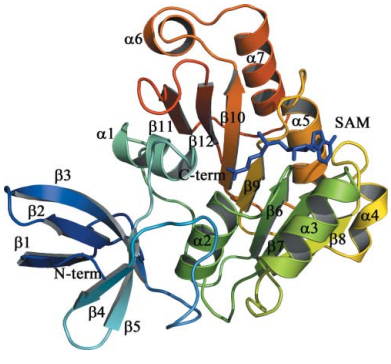

domain that is common to SAM-dependent methyltransferases (Pintard *et al.*, 2000; Wang *et al.*, 2000). Fibrillarin (Nop1p) has been proposed to be the methyltransferase (methylase enzyme) and is responsible for the catalytic activity (Galardi *et al.*, 2002). Consistent with this proposal, it has been shown that archaeal fibrillarin is essential for methylation; mutant proteins with amino-acid replacements in the SAM-binding motif of fibrillarin are still able to assemble into an sRNP complex, but the resulting complexes are defective in methylation activity (Omer *et al.*, 2002). Fibrillarin was subsequently shown to transfer the methyl group from the cofactor SAM to the target RNA (Deng *et al.*, 2004). This reaction requires the precise positioning of the active site of fibrillarin over the specific 2′-hydroxyl group to be methylated. Interestingly, while fibrillarin methylates this functional group in the context of a Watson–Crick base-paired helix (guide/target), it has little dsRNA-binding activity by itself (Omer *et al.*, 2002). This implies that its active site must be precisely positioned through interactions with other components of the RNP complex. In addition, the 2′-hydroxyl moiety where methylation occurs within the target RNA strand lies at the nucleotide paired with the sRNA guide sequence five nucleotides 5′-downstream of either the D or D′ box. This implies that specificity occurs through a ruler-like mechanism in which fibrillarin is correctly positioned over the site of methylation through association with proteins (L7Ae and Nop56/58 in archaeal organisms) that interact with the C/D or C′/D′ box motifs in a highly specific and spatially dependent manner. Given the complex architecture of these RNPs, there are likely to be other structural requirements that confer site-specificity to fibrillarin, which by itself is inherently nonspecific (Hardin & Batey, 2006). To further understand the structure and function of fibrillarin in archaeal C/D box sRNPs, we successfully expressed, purified and crystallized *Aeropyrum pernix* fibrillarin bound to SAM and solved the X-ray crystal structure at 1.7 Å resolution (Fig. 1).

2. Materials and methods

2.1. Cloning, expression and purification

The gene encoding *A. pernix* fibrillarin (NP_148452) was cloned from genomic DNA of *A. pernix* (ATCC) using the forward primer 5′-ATGGCTAGCATGGTTGAGGTTGTAAGCGTTAGAG-3′ and the reverse primer 5′-CGCAAGCTTCTACCTCCTCATAACCGC-GTATATC-3′. The gene was cloned into pET28a vector with a C-terminal His_6 tag (without any linker between the tag and the protein) and expressed in *Escherichia coli* Rosetta2 (DE3) pLysS cells (Novagen). The cells were induced at an OD_{600} of 0.8 with 1 m*M* isopropyl *β*-D-1-thiogalactopyranoside for 4 h at 310 K. Induced cells were resuspended and lysed in 20 m*M* Tris–HCl pH 8.0, 200 m*M* NaCl, 10 m*M* imidazole supplemented with 100 m*M* PMSF, 50 m*M* benzamidine, 1 µg ml^{-1} DNase I and 1 µg ml^{-1} RNase. The sample was centrifuged and the supernatant was processed using the batch method with Ni–NTA resin (Qiagen). The eluted protein was dialyzed into 20 m*M* Tris–HCl pH 8.0, 150 m*M* NaCl and digested with thrombin to remove the His_6 tag. The cleaved protein was further purified using a HiTrap SP Sepharose XL column. The eluted fractions containing pure fibrillarin (Supplementary Fig. S1A[1]) were pooled, dialyzed against 50 m*M* Tris–HCl pH 7.5, 100 m*M* NaCl, 0.5 m*M* EDTA and concentrated to 6.1 mg ml^{-1} (228.5 µ*M*). The homogeneity of the purified protein was examined using dynamic light scattering with a DynaPro plate reader and *DYNAMICS* software (Wyatt).

2.2. Protein crystallization, data collection and data processing

Crystallization trials using His_6-tagged and tag-cleaved *A. pernix* fibrillarin were carried out by the hanging-drop and sitting-drop vapor-diffusion methods with commercially available crystallization screens. Initial protein crystals appeared from hanging drops of His_6-tagged *A. pernix* fibrillarin after 5–7 d at 296 K using a 1:1 ratio of protein to well solution (Supplementary Fig. S1B). The mother liquor consisted of 100 m*M* sodium cacodylate pH 6.5, 200 m*M* Li_2SO_4, 25% PEG 3350, 5% 2-methyl-2,4-pentanediol (MPD). The crystallization conditions were optimized and crystals appeared within 6 h. Optimal conditions included dialysis of the protein into 20 m*M* Tris–HCl pH 8.0, 150 m*M* NaCl, 200 m*M* imidazole and equilibration against a crystallization solution consisting of 20 m*M* Tris–HCl pH 7.0, 5% 2-propanol, 10% PEG 4000. *A. pernix* fibrillarin crystals were flash-cooled in mother liquor containing 10% PEG 4000 as a cryoprotectant. X-ray data were collected on a MicroMax-007 generator with a Saturn 92 CCD detector using Cu *Kα* radiation and the *CrystalClear* software (Rigaku). All data were collected as 0.5° oscillations at a crystal-to-detector distance of 37 mm to reduce superposition of the diffraction spots. A single crystal was used to collect all of the data. Initial exposures of the crystal showed that it diffracted to 2 Å resolution. The diffraction was improved to 1.7 Å resolution after increasing the exposure time, modifying the crystal orientation (κ) and changing the detector orientation (2θ). The crystal was exposed for 60 and 120 s to obtain a 180° ($\kappa = 0°, 2\theta = 0°$) low-resolution (46.3–2.4 Å) data set and a high-resolution (46.3–1.9 Å) data set. Two additional data sets (*i.e.* 2 × 180° of crystal rotation) were collected with 60 and 120 s exposure times at a detector 2θ angle of 7°. One additional data set (180°) was collected with $\kappa = 45°$ and $2\theta = 0°$.

Intensity data were processed, scaled and merged with *d*TREK* (Pflugrath, 1999). The overall completeness was 90.6% with a high

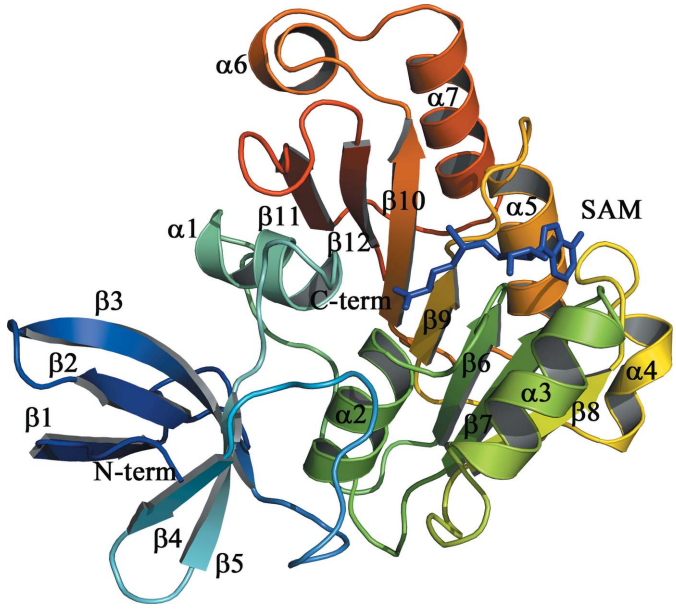

Figure 1
The crystal structure of *A. pernix* fibrillarin bound to the SAM cofactor. The fibrillarin molecule is approximately 48 Å long and 32 Å wide. The N-terminal domain (residues 1–56) consists of five *β*-strands. The C-terminal domain (57–229) consists of seven *β*-strands that are sandwiched between seven *α*-helices. The SAM cofactor is positioned perpendicular to the *β*-sheet of the C-terminal domain.

[1] Supplementary material has been deposited in the IUCr electronic archive (Reference: CB5012).

Table 1
Data-collection and refinement statistics for *A. pernix* fibrillarin.

Values in parentheses are for the highest resolution shell.

Space group	*P*1
Unit-cell parameters (Å, °)	a = 39.64, b = 52.08, c = 63.03, α = 66.3, β = 84.5, γ = 77.6
Crystallographic data statistics	
Resolution (Å)	46.3–1.73 (1.79–1.73)
Solvent content (%)	43.55
Matthews coefficient (Å^3 Da^{-1})	2.18
Reflections	
Total	372034
Unique	42650
Wavelength (Å)	1.54
Temperature (K)	100
Completeness (%)	90.6 (94.0)
Multiplicity	9.1 (7.9)
$R_{\rm merge}$† (%)	6.6 (30.0)
$\langle I/\sigma(I)\rangle$	18.9 (4.6)
Crystal mosaicity (°)	0.98
Crystal-to-detector distance (mm)	37
φ (°)	0.5
Total No. of images	1800
Exposure time per image (s)	120
Refinement statistics	
$R_{\rm free}$‡ (%)	23.35
$R_{\rm cryst}$§ (%)	18.7
Average B factor (Å^2)	
Protein	21.5
Water	29.1
Ligand	19.6
Root-mean-square deviation	
Bond lengths (Å)	0.02
Bond angles (°)	1.35
No. of atoms	
Protein	7438
Solvent	334
Ligand	54
Ramachandran plot analysis (%)	
Most favored region	97.8
Additionally allowed region	2.2
Generously allowed region	0.0
Disallowed region	0.0

† $R_{\rm merge} = \sum_{hkl}\sum_i |I_i(hkl) - \langle I(hkl)\rangle| / \sum_{hkl}\sum_i I_i(hkl)$, where $I_i(hkl)$ is the observed intensity and $\langle I(hkl)\rangle$ is the average intensity. ‡ $R_{\rm cryst} = \sum_{hkl} ||F_{\rm obs}| - |F_{\rm calc}|| / \sum_{hkl} |F_{\rm obs}|$. § $R_{\rm free}$ is the same as $R_{\rm cryst}$ but calculated with 10% of the reflections that were not used for crystallographic refinement.

signal-to-noise ratio that may be a consequence of the constant detector distance used throughout data collection. In addition, there may have also been overlaps at low resolution that caused reduced completeness. The data were re-analyzed with *HKL*-2000 (Otwinowski & Minor, 1997) and *MOSFLM* (Leslie, 1992) in an attempt to identify a higher symmetry unit cell. Nevertheless, *P*1 was determined to be the best-fitting unit cell.

2.3. Structure determination and refinement

Phases for the data were obtained by the molecular-replacement method using *Phaser* (McCoy *et al.*, 2005). The molecular-replacement search model was a composite homology model of *A. pernix* fibrillarin generated using *SWISS-MODEL* (Schwede *et al.*, 2003) based on the structures of *M. jannaschii*, *Archaeoglobus fulgidus* and *Pyrococcus furiosus* fibrillarin. The initial crystallographic model was built using *ARP*/*wARP* (Cohen *et al.*, 2008) and further fitted using *Coot* (Emsley & Cowtan, 2004). Water molecules were added to the model using *Coot* by utilizing the peak strength in a difference electron-density map and the hydrogen-bond lengths between atoms and modified manually as necessary. The structure was refined using *REFMAC*5 (Murshudov *et al.*, 2011), with 10% of the reflections not being used in crystallographic refinement. The changes in the *R* factor and $R_{\rm free}$ were monitored at each step in refinement, in addition to inspection of the stereochemical parameters of the model with *PROCHECK* (Laskowski *et al.*, 1993) and *ERRAT* (Colovos & Yeates, 1993). The model of *A. pernix* fibrillarin converged with a final *R* factor of 18.7% ($R_{\rm free}$ = 23.5%) using all observed X-ray data measurements in the resolution range 46.3–1.73 Å (Table 1). The Ramachandran plot shows that 97.8% of the model residues had φ and ψ angles in the most preferred regions of the plot, with no residues in the disallowed regions. 12 residues were in the additionally allowed regions and none were in the generously allowed regions.

3. Results and discussion

3.1. Overall structure

A. pernix fibrillarin crystallized in space group *P*1 with two molecules in the unit cell. The protein molecules are stacked on each other with active sites oriented towards the same side of the molecules. This dimer formation in the crystal lattice has no apparent biological relevance, as experimentally determined by dynamic light scattering and size-exclusion chromatography. These experiments showed that *A. pernix* fibrillarin has a molecular weight of approximately 26.7 kDa and that it tumbles as a monomer in solution. *A. pernix* fibrillarin has an overall globular structure that consists of two identifiable domains: an N-terminal domain (residues 1–56), which consists of five β-strands, and a larger C-terminal domain (resides 57–229), which consists of seven β-strands sandwiched between seven α-helices (Fig. 1). Only one of the β-strands (β12) is antiparallel. This is a common feature of the *S*-adenosyl-L-methionine-dependent methyltransferase superfamily. The SAM cofactor is located within the C-terminal domain and is positioned perpendicular to the internal β-sheet. The C-terminal residues MRRHHHHHH were not visible in the structure.

Crystals were grown under different conditions (*i.e.* with and without SAM) but led to the same result. A SAM molecule was consistently bound to each of the protein molecules in the crystals obtained under both conditions. It appears that the SAM cofactor is sequestered by the protein during expression in *E. coli* and copurifies and crystallizes as a complex. However, this is contrary to some biochemical evidence, which suggests that SAM may bind weakly to fibrillarin (Aittaleb *et al.*, 2004).

Currently, there are structures of nine archaeal and one eukaryotic fibrillarin proteins in the Protein Data Bank (sequence comparisons of *A. pernix* fibrillarin with these fibrillarin structures are shown in Supplementary Fig. S2). Eukaryotic fibrillarin proteins contain an N-terminal glycine- and arginine-rich (GAR) domain with low sequence complexity that is not present in archaeal fibrillarins. Human fibrillarin is the only eukaryotic fibrillarin structure that has been determined to date (PDB entry 2ipx; Structural Genomics Consortium, unpublished work). When the *A. pernix* fibrillarin structure was compared with structural orthologs the structures differed with r.m.s.d.s of between 3.22 and 5.65 Å, with the structures having an average of 230 C^α atoms per molecule. The predominant variations were observed in the α7, α6 and β10 regions of *A. pernix* fibrillarin.

Three of the known fibrillarin structures, PDB entries 1nt2 (Aittaleb *et al.*, 2003), 3id5 and 3id6 (Ye *et al.*, 2009), contain a SAM cofactor complexed with other RNPs. *A. pernix* fibrillarin is the only structure that contains SAM natively bound to a fibrillarin molecule. It is unusual and interesting to discover that *A. pernix* fibrillarin cocrystallized with SAM. However, the apo structure of *A. pernix* fibrillarin could not be crystallized even with extensive dialysis to remove SAM. It is possible that the binding of the cofactor induced

conformational changes and/or stabilized fibrillarin in a conformation that favored crystallization.

3.2. Ligand-binding and active-site interactions

The structures of several fibrillarin homologs contain analogs of the *S*-adenosyl-L-methionine molecule, but none of them contain a natively bound active SAM molecule. The cocrystal structure of *A. pernix* fibrillarin with SAM revealed that a number of conserved residues interact with the SAM cofactor (Fig. 2). The binding pocket of fibrillarin is surrounded by acidic, nonpolar and polar residues. As shown in the *LIGPLOT* (Wallace *et al.*, 1995) schematic, many fibrillarin residues are involved in hydrogen-bond and hydrophobic interactions with the SAM ligand (Fig. 3). The adenine ring of SAM is stabilized by hydrophobic interactions with Phe110, Ala135 and Val155 and a hydrogen bond to Gln157. The adenine ring of SAM is buried deep in the binding pocket, which prevents exposure to the solvent. Most importantly, the nonpolar residue Phe110 establishes a π–π stacking interaction with the adenine ring of SAM. This interaction is approximately 3.5 Å from the adenine ring and appears to play a critical role in stabilizing the association of the cofactor with fibrillarin. In addition, the ribose moiety of SAM is stabilized by two hydrogen bonds and a hydrophobic interaction with Glu109. The terminal carboxyl group of SAM is oriented by Thr91 using two hydrogen bonds and a hydrophobic interaction.

The crystal structures of fibrillarin and other RNPs from *Sulfolobus solfataricus* (PDB entries 3id6 and 3id5; Ye *et al.*, 2009) and *A. fulgidus* (PDB entry 1nt2; Aittaleb *et al.*, 2003) are the only other structures that contain a SAM cofactor as opposed to a substrate analog. In the *A. pernix* fibrillarin–SAM structure the terminal N atom of SAM forms three hydrogen bonds to Tyr83, Asp154 and Gly85 to stabilize the methionine segment of the molecule. The methyl moiety attached to the SAM methionine sulfur is chemically reactive and is transferred to an acceptor substrate in transmethylation reactions. In the *A. pernix* structure, the methionine sulfur and methyl group do not appear to interact with surrounding active-site residues. However, Asp154 is thought to form hydrogen bonds with the methyl group and amine N atom (Aittaleb *et al.*, 2004; Horowitz *et al.*, 2011). Asp154 is near the methyl group and may reposition when other ribonucleoproteins or RNA bind to fibrillarin.

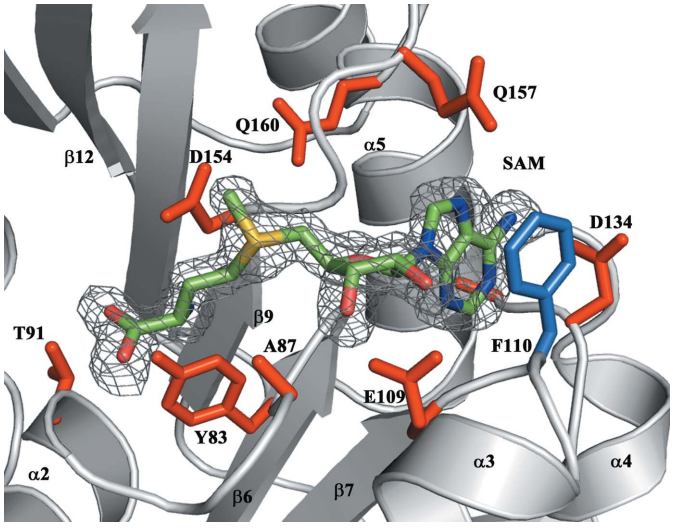

Figure 2
Active site of *A. pernix* fibrillarin. The active-site residues of *A. pernix* with SAM, displaying the cofactor-binding environment. The π–π stacking interaction between the adenine ring of SAM and Phe110 (blue) is clearly visible. Red residues are principally involved in polar interactions and blue residues are involved in hydrophobic interactions. The OMIT electron-density map ($F_o - F_c$) shows the presence of SAM at 1.7 Å resolution with a contour level of 2σ.

3.3. Differences in *A. pernix* fibrillarin helix α6 and Phe110

When *A. pernix* fibrillarin is compared with homologous structures, it is apparent that there are key differences that may play an important role in catalysis, protein–protein interaction and cofactor and RNA binding. A primary difference is the conformational change in helix α6 as shown in Fig. 4(*a*). The least observed conformation, as observed in *A. pernix* fibrillarin helix α6, is shown as an orange helix and the alternate conformation that is observed in other homologs is shown as a blue helix; the difference in orientation is about 20 Å at the furthest points considered. In all of the structural homologs that were compared, helix α6 contains a conserved charged amino acid (Supplementary Fig. S2) and is believed to be important for RNA binding. The structure of *S. solfataricus* fibrillarin (PDB entry 3pla; Lin *et al.*, 2011) is in a complex of RNPs and C/D guide RNAs and shows helix α6 in an alternate orientation. This enables *S. solfataricus* fibrillarin α6 to interact with the C/D box RNA. This is the only example in which fibrillarin helix α6 shows a direct interaction with C/D RNA. A conformation similar to that of *A. pernix* fibrillarin α6 is only observed in the 3id5 and 3id6 structures (Ye *et al.*, 2009). Even though the 3id5 structure contains C/D box RNA, the RNA is not near fibrillarin α6 and does not appear to form any interactions. The

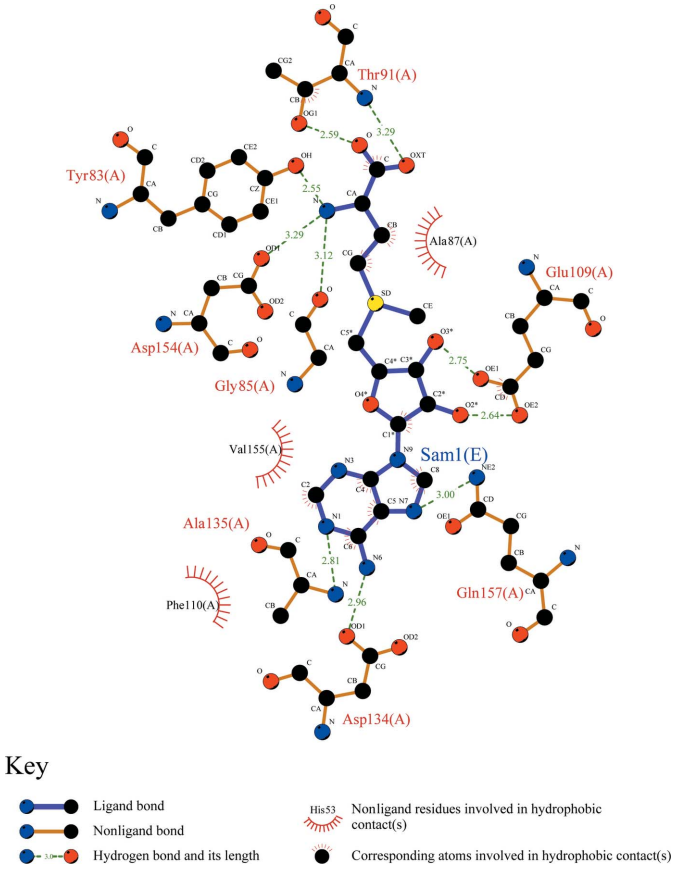

Figure 3
Interactions of *S*-adenosyl-L-methionine with *A. pernix* fibrillarin. *LIGPLOT* schematic of fibrillarin–SAM interactions. Hydrogen-bond lengths are shown in green. Hydrophobic interactions with specific atoms are shown in red as depicted in the key.

alternate conformation of helix α6 (*i.e.* the blue-colored helix in Fig. 4*a*) may result from the close proximity of SAM and RNA in the snRNP complex.

The second key difference is the π–π stacking interaction between SAM and Phe110, which is located in the α3–β7 region. In Fig. 4(*b*) the green peptide represents the α3–β7 region of *A. pernix* fibrillarin and highlights the movement of Phe110. A comparison of homologous structures suggests that when SAM is present in the structure Phe110 is in close proximity to the adenine ring. Most of the fibrillarin homologs contain a phenylalanine at this position, with the exception of PDB entries 1nt2 (*A. fulgidus*; Aittaleb *et al.*, 2003) and 1g8s (*M. jannaschii*), both of which contain a tyrosine in this position. The π–π stacking interaction brings the adenine ring and phenylalanine/tyrosine into close proximity (∼3.6 Å). The alternate conformation orients this aromatic residue approximately 1.8 Å away from the stacking position. The aromatic amino acid–adenine ring stacking interaction is observed in all fibrillarin structures containing SAM except for the *S. solfataricus* protein complexes (PDB entries 3id5 and 3id6; Ye *et al.*, 2009). In these structures the phenylalanine residue swings away from the adenine ring. Overall, the π–π stacking orientation appears to be the preferred conformation and may be an important interaction for positioning the SAM cofactor during catalysis.

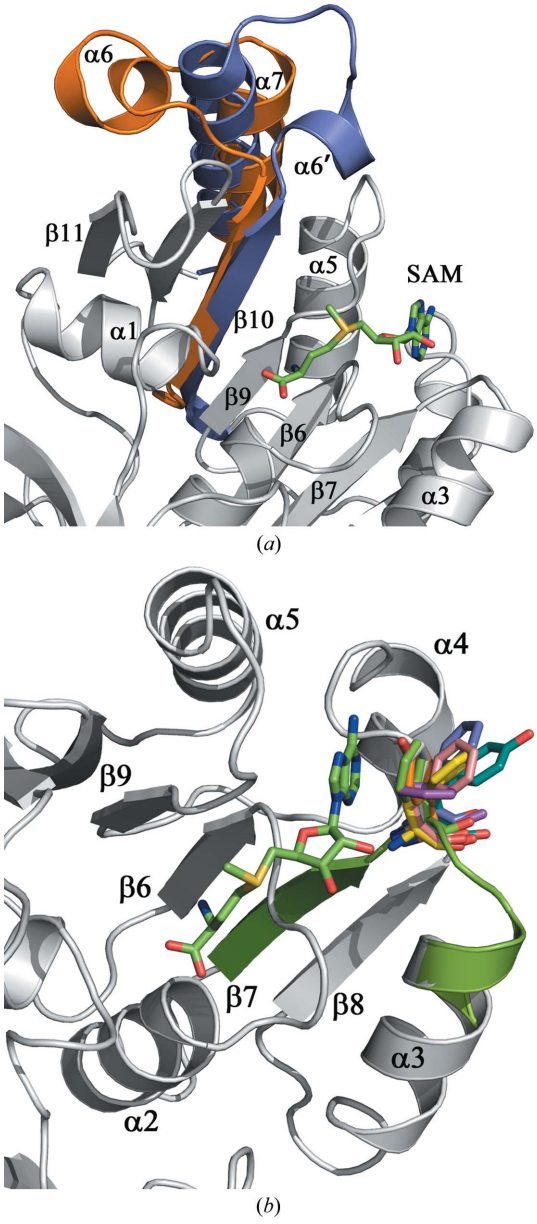

Figure 4
Variations in helix α6 and Phe110 relative to SAM. (*a*) Movement of helix α6 relative to SAM. The orange peptide orientation is that in *A. pernix* fibrillarin and the blue peptide orientation occurs when fibrillarin homologs are complexed with other RNPs and may be important for protein–RNA interaction. (*b*) π–π stacking interaction between SAM and Phe110. The different orientations of the aromatic residues from fibrillarin homologs that are relevant to π–π stacking interactions are shown. Green, *Aeropyrum pernix*; gray, *Homo sapiens*; purple, *Saccharomyces cerevisiae*; salmon, *Pyrococcus furious*; dark green, *Methanococcus jannaschii*; yellow, *Sulfolobus solfataricus*; orange, *Archaeoglobus fulgidus*.

4. Conclusion

The high-resolution structure describes the first natively bound SAM molecule in fibrillarin by itself (Fig. 5). When sequences of fibrillarin homologs were compared using a phylogram, the branch lengths suggested that *A. pernix* fibrillarin is similar to an ancestral fibrillarin molecule (Supplementary Fig. S3). The structure of *A. pernix* fibrillarin shows many molecular interactions involving the SAM cofactor. The *A. pernix* fibrillarin structure also shows an alternative orientation of the α6 helix. Comparison of homologous structures with *A. pernix* fibrillarin shows that the α6 helix may play a role in protein–RNA interactions. The movement of the π–π stacking Phe110 in the α3–β7 region may represent a gating mechanism that is utilized by fibrillarin to orient and shuttle SAM in and out of the active site for

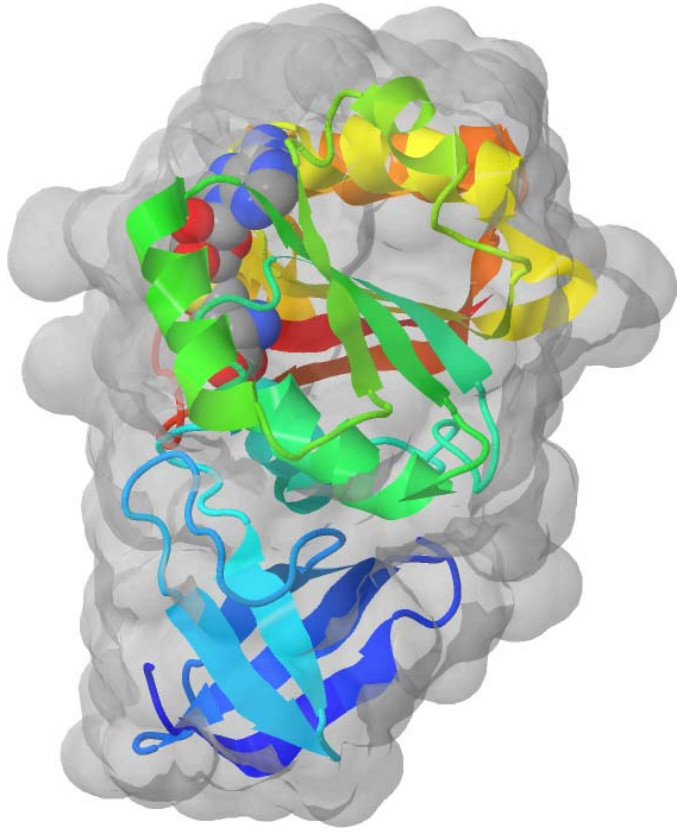

Figure 5
Structure of *A. pernix* fibrillarin in complex with natively bound *S*-adenosyl-L-methionine at 1.7 Å.

catalysis. Since we did not obtain crystals of *A. pernix* fibrillarin without SAM, it was not possible to determine the molecular changes that occur upon SAM binding. However, comparisons between the published fibrillarin apo structures and *A. pernix* fibrillarin suggest that Phe110, together with other active-site residues, plays a key role in orienting the SAM ligand in the active site.

We would like to thank Dr David R. Davies of National Institutes of Health for proofreading the manuscript and NIH/NIDDK/LMB for their generous support with computer resources. This research was supported in part by National Institutes of Health Grant GM069699 to BAB. This research was initiated in the Department of Chemistry, Wake Forest University (ZZ and BAB) and the Department of Biochemistry, Wake Forest University School of Medicine (UdS).

References

Aittaleb, M., Rashid, R., Chen, Q., Palmer, J. R., Daniels, C. J. & Li, H. (2003). *Nature Struct. Biol.* **10**, 256–263.
Aittaleb, M., Visone, T., Fenley, M. O. & Li, H. (2004). *J. Biol. Chem.* **279**, 41822–41829.
Caffarelli, E., Losito, M., Giorgi, C., Fatica, A. & Bozzoni, I. (1998). *Mol. Cell. Biol.* **18**, 1023–1028.
Cohen, S. X., Ben Jelloul, M., Long, F., Vagin, A., Knipscheer, P., Lebbink, J., Sixma, T. K., Lamzin, V. S., Murshudov, G. N. & Perrakis, A. (2008). *Acta Cryst.* D**64**, 49–60.
Colovos, C. & Yeates, T. O. (1993). *Protein Sci.* **2**, 1511–1519.
Deng, L., Starostina, N. G., Liu, Z.-J., Rose, J. P., Terns, R. M., Terns, M. P. & Wang, B.-C. (2004). *Biochem. Biophys. Res. Commun.* **315**, 726–732.
Eichler, D. C. & Craig, N. (1994). *Prog. Nucleic Acid Res. Mol. Biol.* **49**, 197–239.
Emsley, P. & Cowtan, K. (2004). *Acta Cryst.* D**60**, 2126–2132.
Galardi, S., Fatica, A., Bachi, A., Scaloni, A., Presutti, C. & Bozzoni, I. (2002). *Mol. Cell. Biol.* **22**, 6663–6668.
Hardin, J. W. & Batey, R. T. (2006). *Nucleic Acids Res.* **34**, 5039–5051.
Horowitz, S., Yesselman, J. D., Al-Hashimi, H. M. & Trievel, R. C. (2011). *J. Biol. Chem.* **286**, 18658–18663.
Laskowski, R. A., MacArthur, M. W., Moss, D. S. & Thornton, J. M. (1993). *J. Appl. Cryst.* **26**, 283–291.
Leslie, A. G. W. (1992). *Jnt CCP4/ESF–EACBM Newsl. Protein Crystallogr.* **26**.
Lin, J., Lai, S., Jia, R., Xu, A., Zhang, L., Lu, J. & Ye, K. (2011). *Nature (London)*, **469**, 559–563.
McCoy, A. J., Grosse-Kunstleve, R. W., Storoni, L. C. & Read, R. J. (2005). *Acta Cryst.* D**61**, 458–464.
Murshudov, G. N., Skubák, P., Lebedev, A. A., Pannu, N. S., Steiner, R. A., Nicholls, R. A., Winn, M. D., Long, F. & Vagin, A. A. (2011). *Acta Cryst.* D**67**, 355–367.
Newton, K., Petfalski, E., Tollervey, D. & Cáceres, J. F. (2003). *Mol. Cell. Biol.* **23**, 8519–8527.
Omer, A. D., Ziesche, S., Ebhardt, H. & Dennis, P. P. (2002). *Proc. Natl Acad. Sci. USA*, **99**, 5289–5294.
Otwinowski, Z. & Minor, W. (1997). *Methods Enzymol.* **276**, 307–326.
Pflugrath, J. W. (1999). *Acta Cryst.* D**55**, 1718–1725.
Pintard, L., Kressler, D. & Lapeyre, B. (2000). *Mol. Cell. Biol.* **20**, 1370–1381.
Schwede, T., Kopp, J., Guex, N. & Peitsch, M. C. (2003). *Nucleic Acids Res.* **31**, 3381–3385.
Wallace, A. C., Laskowski, R. A. & Thornton, J. M. (1995). *Protein Eng.* **8**, 127–134.
Wang, H., Boisvert, D., Kim, K. K., Kim, R. & Kim, S.-H. (2000). *EMBO J.* **19**, 317–323.
Ye, K., Jia, R., Lin, J., Ju, M., Peng, J., Xu, A. & Zhang, L. (2009). *Proc. Natl Acad. Sci. USA*, **106**, 13808–13813.